東北大学機関リポジトリ
TOUR
Tohoku University Repository

# Evaluation of the reactivity of ultra-lean PRF/air mixtures by weak flames in a micro flow reactor with a controlled temperature profile

# Evaluation of the reactivity of ultra-lean PRF/air mixtures by weak flames in a micro flow reactor with a controlled temperature profile

P. Grajetzki[a], H. Nakamura[a], T. Tezuka[a], S. Hasegawa[a] and K. Maruta[a,b]

[a]Institute of Fluid Science, Tohoku University, Japan

[b]International Combustion and Energy Laboratory, Far Eastern Federal University, Russia

CONTACT P. Grajetzki. Email: grajetzki@edyn.ifs.tohoku.ac.jp

**ABSTRACT**

The reactivity of ultra-lean PRF/air mixtures was investigated by weak flames in a vertical-type micro flow reactor with a controlled temperature profile. In experiments, steady-separated weak flames were obtained at equivalence ratios between 0.5 and 1.0 for PRF80, 90 and 100. At leaner conditions, all the fuels showed hot flames at lower temperature regions, indicating higher reactivity. In 1-D steady simulations of the present micro flow reactor by modified Chemkin-Pro PREMIX, the LLNL PRF mechanism was able to reproduce the experimental tendency, while the KUCRS PRF mechanism showed the opposite trend. By analyzing major reactions leading to the hot flame, seven H-O reactions were identified that primarily control the hot flame response to a change of equivalence ratio. By exchanging the rate parameters of these seven reactions for more recent ones, the reactivity trend was brought to very good agreement with experimental results. This improvement was credited to a better spatial separation of intermediate and high temperature reactions in the MFR and emphasizes the strength of this investigation method.

**KEYWORDS**

## 1. Introduction

In the ongoing task of increasing the thermal efficiency of automotive engines, gasoline combustion under ultra-lean conditions is an approach with high potential (Bradley et al., 2000). On the other hand, achieving well-controlled ignition and combustion under these conditions have not been well understood yet, and pose a major problem for commercial application. To address this challenge, the Japanese government launched the *Cross-ministerial Strategic Innovation Promotion Program* (SIP program) in cooperation with all major Japanese car manufacturers and more than fifty universities in 2014 (SIP, 2015). The project aims to increase the thermal efficiency of gasoline engines to 50 % in 2019 by, among others, using ultra-lean combustion (equivalence ratio $\Phi = 0.5$). In this process, gasoline surrogates that match Japanese gasoline with regard to chemical and physical properties are being developed as a secondary goal. In order to analyze the occurring chemical reactions in the combustion of these surrogates, detailed reaction mechanisms are being created and validated in this process (Miyoshi and Sakai, 2017).

To obtain fundamental ignition data for mechanism validation of lean combustion of primary reference fuels (PRF), past researches mainly employed shock tubes (Mehl et al., 2011; Gauthier et al., 2004; Andrae et al., 2007; Sarathy et al., 2015; Hartmann et al., 2011; Javed et al., 2016; AlAbbad et al., 2017), rapid compression machines (RCM) (Mehl et al., 2011; Sarathy et al., 2015; Javed et al., 2016) and jet-stirred reactors (JSR) (Curran et al., 2002; Chen et al., 2017). Shock tubes were used to investigate ignition delay times (IDTs) at higher temperatures. At pressures around 10 atm, IDTs decreased with decreasing equivalence ratio. This indicated a higher reactivity in leaner conditions (Sarathy et al., 2015). At higher pressures, shock tubes (Gauthier et al., 2004; Sarathy et al., 2015) as well as RCMs (Kukkadapu et al., 2012, 2015) showed longer IDTs with decreasing equivalence ratio, indicating lower reactivity.

The present study employs a novel investigation method, the micro flow reactor with a controlled temperature profile (MFR) (Maruta et al., 2005; Minaev et al., 2007). It allows for the investigation of ignition characteristics of low reactivity fuels and mixtures. It was introduced by our group in 2005 and has since been used by other groups

as well (Saiki and Suzuki, 2013; Saiki et al., 2015; Di Stazio et al., 2016). The MFR consists of a quartz tube with an inner diameter that is smaller than the ordinary quenching diameter. It is heated by an external heat source and a stationary wall temperature profile is formed in the axial direction on the quartz tube's inner surface. Fuel/oxidizer mixtures are supplied at the cold side. In general, the gas-phase temperature is strongly governed by the given wall temperature profile inside the MFR. Depending on the inlet flow velocity, three types of flame responses are observed. At high flow velocities, a bright stable flame appears. It is called *normal flame* and represents flame propagation of a preheated mixture. In the intermediate flow velocity regime, an oscillating flame, called *FREI* (Flame with Repetitive Extinction and Ignition), occurs. It ignites at a high temperature location and propagates upstream to lower temperatures where it extinguishes before the fresh mixture ignites again at high temperature and starts a new cycle. At very low flow velocities another stable flame appears. It has a very low heat release and shows very low luminosity, which can only be seen by long exposure photography. Due to its low heat release, it raises the gas-phase temperature at the flame location less than $30\,\mathrm{K}$ above the prescribed temperature profile, depending on the flow velocity and the equivalence ratio (Tsuboi et al., 2009). Based on theoretical basis, this flame was identified as a stable solution of the Fendel curve, where it represents this curve's ignition branch (Minaev et al., 2007). This flame is called *weak flame* (Maruta et al., 2005). Weak flames have been used to study ignition characteristics of various fuels, such as methane (Maruta et al., 2005; Tsuboi et al., 2009; Li et al., 2015; Okuno et al., 2017), butane (Kikui et al., 2015), $n$-heptane (Yamamoto et al., 2011), DME (Oshibe et al., 2010), ethanol (Nakamura et al., 2013), lower alkenes (Kikui et al., 2016) and mixtures such as PRF (Hori et al., 2012) and TRF (Hori et al., 2013). For weak flames of fuels with higher carbon number, it was found that the flame spatially separates in up to three distinct and stable reaction zones. These reaction zones correspond to the *cool flame* at low wall temperatures, the *blue flame* at intermediate temperatures and the *hot flame* at high wall temperatures, respectively. This particular characteristic of the reaction separation allows for the study of occurring reactions in high detail as it is time independent. Furthermore, the effect of radical quenching on the flame location was
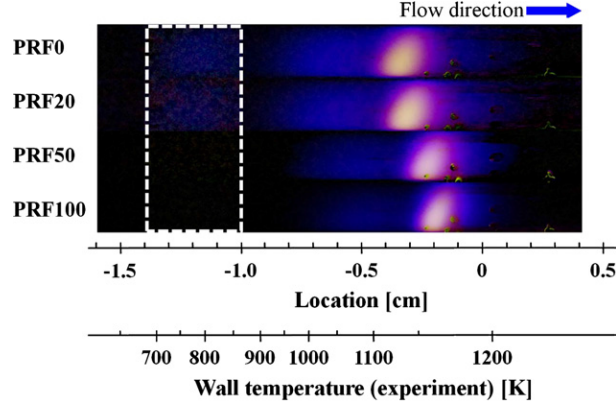
4

**Figure 1.** Influence of RON on flame patterns and positions at $\Phi = 1.0$, $P = 1$ atm, horizontal-type MFR (Hori et al., 2012). Flame regions from left to right: cool flame, blue flame, hot flame.

shown to be negligible (Saiki and Suzuki, 2013; Saiki et al., 2015; Kizaki et al., 2015).

By comparing the research octane numbers (RON) of the investigated fuels, a correlation between RON and the weak flame response becomes evident. Figure 1 shows the experimental weak flame images of several PRFs at stoichiometry and atmospheric pressure. Fuels with RON between 20 and 100 show blue flames at intermediate temperatures and hot flames at high temperatures. As the RON is decreased, these flames shift to lower temperatures. The cool flame is only visible for RON less than 20, as these fuels show strong low temperature oxidization (LTO). In the investigation of ultra-lean methane weak flames, it was found that the hot flames moved to lower wall temperatures for lower equivalence ratios (Okuno et al., 2017).

The goal of this study is to investigate the reactivity of ultra-lean PRF/air mixtures ($\Phi = 0.5$, 0.75, 1.0) by weak flames. PRF100, PRF90 and PRF80 were chosen as fuels as they show similar reactivities as actual gasoline fuels. The broad temperature profile af the vertical-type MFR yields a high resolution with regard to location and temperature and allows for a precise distinction between different weak flame responses. The experimental results can then be used for the validation of the KUCRS reaction mechanism, which is the base mechanism of the SIP project.
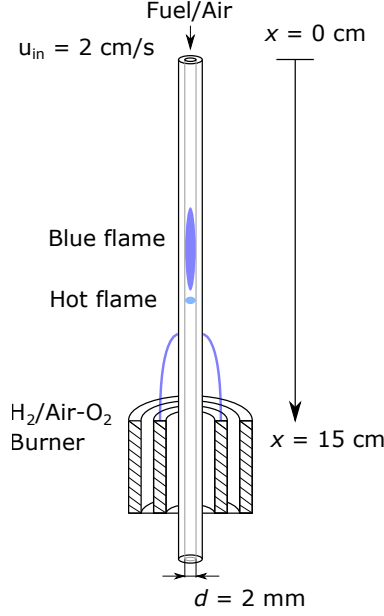
5

Figure 2. Scheme of the vertical-type micro flow reactor with a controlled temperature profile.

## 2. Methods

### 2.1. Experimental method

In this study, PRF100, PRF90 and PRF80, i.e., mixtures of *iso*-octane and *n*-heptane (100:0, 90:10 and 80:20 by liquid volume fraction), were investigated with regard to their reactivity at stoichiometric to ultra-lean conditions ($\Phi = 1.0$, 0.75 and 0.5). For this task, a vertical-type MFR was developed as part of this study (see Figure 2). It consists of a vertical quartz tube with a length of 15 cm and an inner diameter of 2 mm. Around the bottom end, a coaxial $H_2/O_2$-enriched-air non-premixed burner was attached as the external heat source, which led to a mildly increasing temperature profile between the top to the bottom. This allows for an increased temperature resolution in the axial direction as compared to the horizontal type, which was used in previous studies (Oshibe et al., 2010; Kamada et al., 2014; Kikui et al., 2016). Furthermore, the usage of an annular burner ensures an axisymmetric temperature profile in the radial direction. The temperature profile along the inner surface of the tube was measured by a sheathed K-type thermocouple with a diameter of 300 $\mu$m that was inserted into the tube from the lower end before and after the experiments. In previous trials, we conducted measurements with sheath-type thermocouples with diameters of 320 $\mu$m
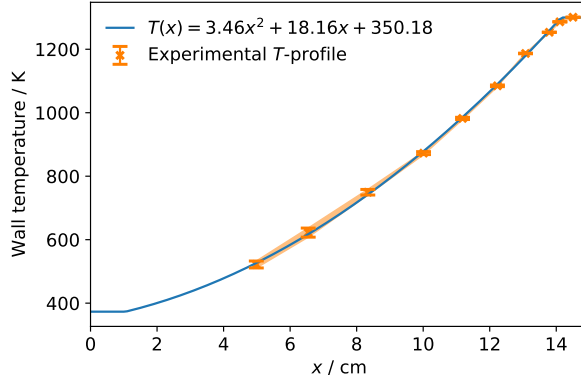
6

**Figure 3.** Experimentally measured wall temperatures and fitted quadratic function between $373\,\mathrm{K}$ and $1300\,\mathrm{K}$.

and $160\,\mu\mathrm{m}$ as well as with bare wires down to a diameter of $50\,\mu\mathrm{m}$. For temperatures up to 1200 K, the differences between the different types were negligible. The tip of the thermocouple was in direct contact with the inner wall surface and was held in each position for several minutes to obtain the average temperature and its fluctuation at each measurement point. The axial location was analyzed by digital image processing with an uncertainty of less than $100\,\mu\mathrm{m}$. Due to the small inner diameter of the tube and the direct contact between the thermocouple and the wall, the measured temperature can be assumed to be the actual wall temperature at each point. The temperature profile is shown in Figure 3 with its temporal standard deviation. The temperature inside the tube ranged from $373\,\mathrm{K}$ to $1300\,\mathrm{K}$ and the standard deviation at temperatures of interest for this study, i.e. between $1000\,\mathrm{K}$ and $1100\,\mathrm{K}$, is less than $3\,\mathrm{K}$. From this profile, a quadratic function was fitted that was later used in the simulations. The flow inside the tube was laminar and at atmospheric pressure.

In order to vaporize the liquid fuels, they were introduced into a heated and vacuumed tank ($373\,\mathrm{K}$ at pressures less than $0.25\,\mathrm{kPa}$), where they were mixed with nitrogen by the partial pressure method. The mixture was stored in the tank to ensure complete evaporation of the liquid fuels and uniform mixing with nitrogen. It was then sent to the top inlet of the quartz tube through a heated pipe and a heated mass flow controller at a temperature of $373\,\mathrm{K}$ to prevent condensation of the fuel. On the way, it was mixed with oxygen whose flow rate was controlled by a digital mass flow controller in accordance with equivalence ratios and the $O_2/N_2$ ratio of air. To obtain

**Table 1.** Experimental conditions.

| Parameter | Value |
| --- | --- |
| Fuels | PRF100, 90, 80 |
| *iso*-octane/*n*-heptane ratio | 100:0, 90:10, 80:20 |
| Research octane number (RON) | 100, 90, 80 |
| Equivalence ratio $\Phi$ | 1.0, 0.75, 0.5 |
| Pressure | 1.0 atm |
| MFR length | 15.0 cm |
| Inner diameter | 2.0 mm |
| Temperature range | 373 K to 1300 K |
| Inlet velocity | 2 cm/s (at 373 K) |

weak flames, the inlet velocity of the mixture at the upper end of the tube (at 373 K) was set to 2 cm/s. In previous studies, it was shown that the peak position in the CH chemiluminescence profile agrees well with the peak in the heat release rate profile of the separated weak flames (Tsuboi et al., 2009; Oshibe et al., 2010; Yamamoto et al., 2011; Hori et al., 2012). Therefore, images of the weak flames were taken at exposure times of 100 seconds through a CH band-pass filter (transparent wavelength 432.3 nm, half band width 6.4 nm) by a Nikon D800 still camera. For each case, the intensity of luminosity of five images was averaged and a background subtraction was performed to obtain only the flame. The location of the hot flame, and therefore the wall temperature, was defined as the point of the maximum luminosity. An overview of the experimental conditions is given in Table 1.

## 2.2. Computational method

To evaluate the occurring chemical reactions, one-dimensional steady computations were performed for the three fuels and their respective equivalence ratios. Modified Chemkin-Pro PREMIX (ANSYS, 2016) was used for simulations. For the MFR simulation, an additional term that accounts for the convective heat transfer between the inner surface of the quartz tube and the gas phase was added to the energy equation

(see Eq. 1) as part of a user defined sub-routine (Maruta et al., 2005).

$$\dot{M}\frac{\mathrm{d}T}{\mathrm{d}x} - \frac{1}{c_p}\frac{\mathrm{d}}{\mathrm{d}x}\left(\lambda A\frac{\mathrm{d}T}{\mathrm{d}x}\right) + \frac{A}{c_p}\sum_{k=1}^{K}\rho Y_k V_k c_{p,k}\frac{\mathrm{d}T}{\mathrm{d}x}$$
$$+\frac{A}{c_p}\sum_{k=1}^{K}\dot{\omega}_k h_k W_k - \frac{A}{c_p}\frac{4\lambda Nu}{d^2}(T_{\mathrm{w}} - T) = 0 \tag{1}$$

The wall temperature profile $T_{\mathrm{w}}$ was expressed by the quadratic equation obtained from the experiment (see Figure 3).

The inlet flow velocity was set to $2\,\mathrm{cm/s}$ at $373\,\mathrm{K}$, according to the experiment. Furthermore, the computation domain was $15\,\mathrm{cm}$ and the pressure was $1\,\mathrm{atm}$. Two detailed reaction mechanisms were chosen in this study. LLNL PRF (Curran et al., 2002) is a well established PRF mechanism with 1034 species and 4206 reactions. KUCRS (Miyoshi, 2011) was chosen as it is the base mechanism for more complex gasoline surrogates of the SIP project (Miyoshi and Sakai, 2017). It consists of 778 species and 2181 reactions. The location of the hot flame was defined as the location of maximum heat release rate.

## 3. Results and discussion

### 3.1. Flame locations and temperatures

Images of the weak flames for all three fuels and all three equivalence ratios are shown in Figure 4. The hot flames are clearly visible as the bright spots on the right side at wall temperatures between $1050\,\mathrm{K}$ and $1070\,\mathrm{K}$. The blue flames are located to their left, at wall temperatures between $900\,\mathrm{K}$ and $1050\,\mathrm{K}$. As the RON is lowered from 100 to 80 (PRF100 to PRF80), the hot flame position shifts to the left, i. e., to lower wall temperatures. The shift corresponds to approximately $3\,\mathrm{K}$ per $\Delta\mathrm{RON} = 10$, starting at $1070\,\mathrm{K}$ for PRF100 and $\Phi = 1.0$. A decrease of the equivalence ratio shows the hot flame shifting to the lower wall temperature side by approximately $4\,\mathrm{K}$ for $\Delta\Phi = 0.25$. The shift of the hot flames to lower temperatures indicates higher reactivity. In addition, the intensity of the hot flame, as well as the length of the blue flame decrease with decreasing equivalence ratio. This effect is caused by the lower fuel flux into the system
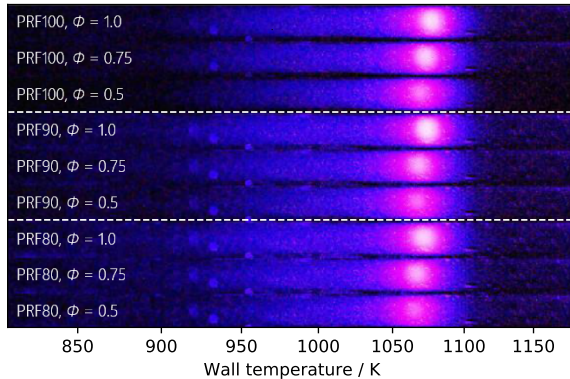
9

**Figure 4.** Experimental weak flame images of all nine cases. Flow direction from left to right.

for lower equivalence ratios.

The computational heat release rate (HRR) profiles by LLNL and KUCRS for PRF100 at $\Phi = 1.0$, 0.75 and 0.5 are shown in Figure 5. Both mechanisms show broad regions of HRR between 850 K and 1050 K and peaks between 1050 K and 1100 K. These represent the blue flames and the hot flames, respectively. For the LLNL mechanism, a decrease of equivalence ratio leads to a shift of the HRR peak, and therefore a shift of hot flame, to lower temperatures, from 1079 K at $\Phi = 1.0$ to 1071 K at $\Phi = 0.5$. This trend agrees with the experimental trend as it shows higher reactivity in leaner conditions. In the case of KUCRS, however, the hot flame moves to higher temperatures, from 1066 K at $\Phi = 1.0$ to 1080 K at $\Phi = 0.5$. This shows lower reactivity at lower equivalence ratios, which is opposite to the experimental results and the computational results with LLNL. Both mechanisms show a decrease of the maximum HRR in the blue flame as well as the hot flame with decreasing equivalence ratio. The wall temperatures at the hot flame location for all investigated cases, experimentally and numerically, are plotted in Figure 6. For PRF80 and PRF90, the same trends as for PRF100 are seen in the simulations. As equivalence ratio decreases, the HRR peaks shift to lower temperatures for LLNL and to higher temperatures for KUCRS. In comparison with PRF100, the hot flames are located at lower wall temperatures as the RON was decreased from 100 to 80 for all the cases. The shift is about 3 K per $\Delta$RON $= 10$, which agrees well with the experimental RON dependence of hot flame locations in this study. In a previous study by Hori et al. (Hori et al., 2012), stoi-
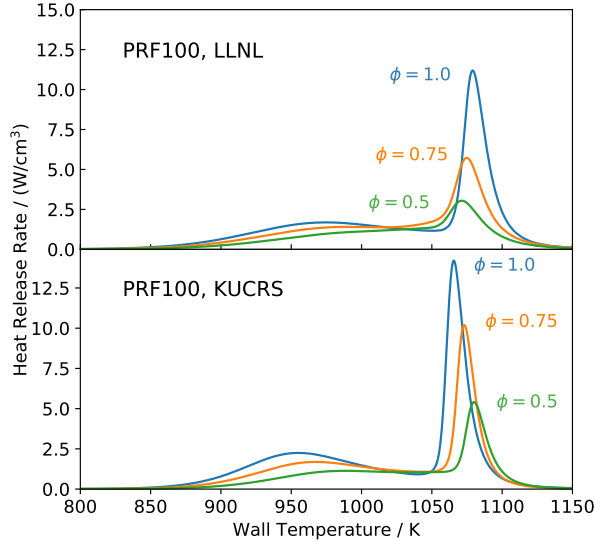
**Figure 5.** Heat release rates of PRF100 with LLNL and KUCRS at $\Phi = 1.0$, 0.75 and 0.5.

chiometric PRF mixtures showed a similar trend with regard to the change of RON. However, due to the usage of the horizontal-type MFR in the previous study, it was only possible to distinguish large differences in RON, as the temperature resolution in the previous study (approximately $5\,\mathrm{K}$) was lower than the temperature difference for $\Delta\mathrm{RON} = 10$ (between $3\,\mathrm{K}$ and $4\,\mathrm{K}$) in the present study.

To understand the structure of the separated weak flames, Figure 7 shows the mole fraction profiles of major species for PRF100 at $\Phi = 1.0$ for weak flame conditions as obtained by LLNL. The region between $600\,\mathrm{K}$ and $700\,\mathrm{K}$ is called cool flame. Fuel consumption by low temperature oxidization (LTO) takes place in this region and intermediate species, such as $CH_2O$, are produced. The next reaction zone is located between $850\,\mathrm{K}$ and $1000\,\mathrm{K}$ and is called the blue flame. In this reaction zone, the remaining fuel and great parts of intermediate species are consumed and CO is formed as the main product. The third zone lies between $1000\,\mathrm{K}$ and $1100\,\mathrm{K}$ and is named hot flame. Here, the CO is oxidized to the final product $CO_2$.

### 3.2. Effect of equivalence ratio on chemical reactions

Figure 8 shows the ten strongest reactions of LLNL for PRF100 and $\Phi = 1.0$ just before the hot flame at $T_{\mathrm{wall}} = 1030\,\mathrm{K}$, and the corresponding values at $\Phi = 0.5$. The
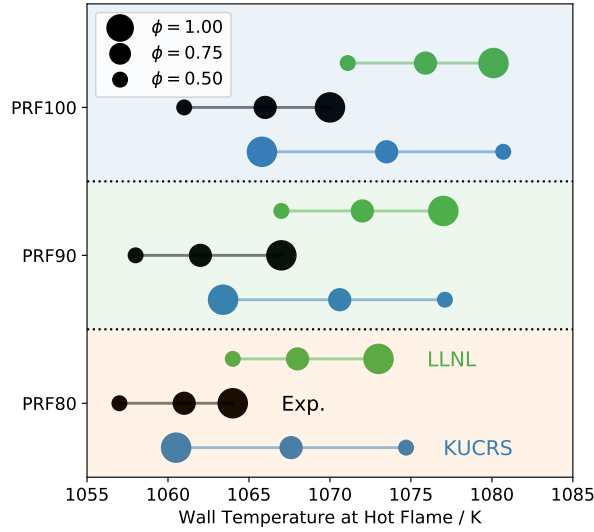
11

**Figure 6.** Wall temperature at hot flame location for all investigated cases, experiments and simulations.
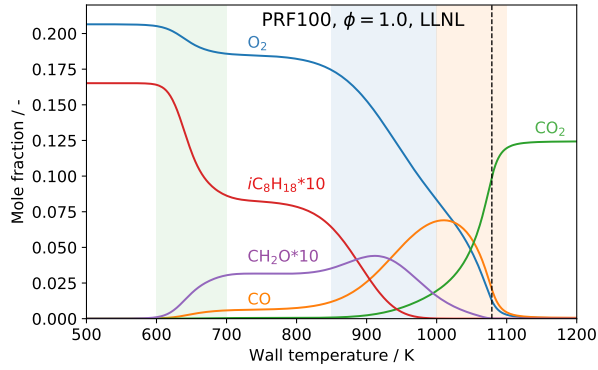


**Figure 7.** Major species profiles for PRF100, $\Phi = 1.0$, LLNL. The vertical dashed line indicates the position of the HRR peak of the hot flame. The colored boxes indicate from left to right the approximate location of the cool flame, blue flame and the hot flame.

wall temperature of 1030 K was chosen as the HRRs at $\Phi = 1.0$ and $\Phi = 0.5$ show opposing trends in this point, where the HRR at $\Phi = 1.0$ is decreasing and that at $\Phi = 0.5$ is increasing towards the hot flame. The rate of progress variables of these ten reactions were normalized by that of L7 (CO oxidization) for each $\Phi$, as this is the dominant reaction in the hot flame. Here, L46 (HCO consumption) is the strongest reaction at both equivalence ratios and it is significantly stronger at $\Phi = 1.0$ than at $\Phi = 0.5$. Other reactions including C1 species, such as L32 ($CH_2O$ consumption), L40 ($CH_3O$ consumption), L22 ($CH_3$ consumption) and L33 ($CH_2O$ consumption) also
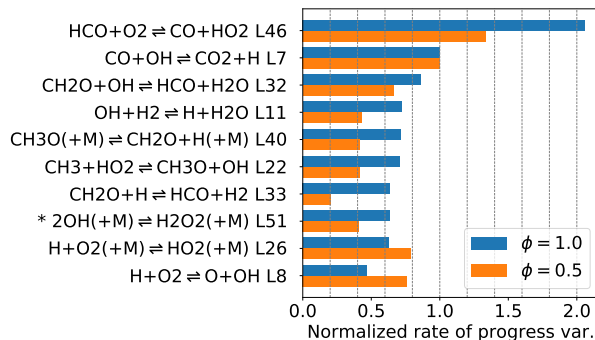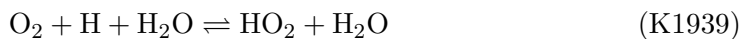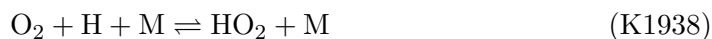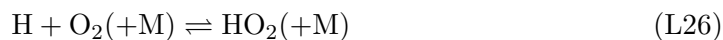
12

**Figure 8.** Normalized rate of progress variable (by $CO + OH \rightleftharpoons CO_2 + H$) at $T_{wall} = 1030\,K$ for major ten reactions of LLNL, PRF100, $\Phi = 1.0$ and corresponding values at $\Phi = 0.5$. *net reaction rate is from right to left.

show higher contribution at $\Phi = 1.0$ than at $\Phi = 0.5$.

$$HCO + O_2 \rightleftharpoons CO + HO_2 \tag{L46/K1982}$$

$$CO + OH \rightleftharpoons CO_2 + H \tag{L7/K1959}$$

$$CH_2O + OH \rightleftharpoons HCO + H_2O \tag{L32/K1970}$$

$$CH_3O(+M) \rightleftharpoons CH_2O + H(+M) \tag{L40}$$

$$CH_3O + M \rightleftharpoons CH_2O + H + M \tag{K1978}$$

$$CH_3 + HO_2 \rightleftharpoons CH_3O + OH \tag{L22/K1963}$$

$$CH_2O + H \rightleftharpoons HCO + H_2 \tag{L33/K1971}$$

On the other hand, rates of progress for reactions of the hydrogen-oxygen system, such as L26 and L8, are higher at $\Phi = 0.5$ than those at $\Phi = 1.0$.

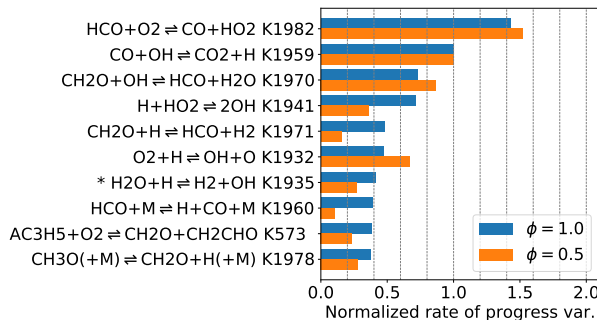$$H + O_2(+M) \rightleftharpoons HO_2(+M) \tag{L26}$$

$$O_2 + H + M \rightleftharpoons HO_2 + M \tag{K1938}$$

$$O_2 + H + H_2O \rightleftharpoons HO_2 + H_2O \tag{K1939}$$

$$H + O_2 \rightleftharpoons O + OH \tag{L8}$$

$$O_2 + H \rightleftharpoons OH + O \tag{K1932}$$

**Figure 9.** Normalized rate of progress variable (by $CO + OH \rightleftharpoons CO_2 + H$) at $T_{wall} = 1053\,K$ for major ten reactions of KUCRS, PRF100, $\Phi = 1.0$ and corresponding values at $\Phi = 0.5$. *net reaction rate is from right to left.

As these H-O reactions include the important chain-branching reaction L8, they promote reactivity. However, these reactions compete with intermediate species for radicals, especially H radicals. As the reactions of intermediate species show lower reactivity in the lean case, the chain branching reaction L8 is enhanced and the hot flame shifts to lower wall temperatures for leaner conditions, which is in agreement with the experimental results.

For KUCRS, the point of diverging HRR profiles is around $T_{wall} = 1053\,K$. Similar to LLNL, the rate of progress variables are normalized by the CO oxidization reaction K1959. The ten strongest reactions of KUCRS are shown in Figure 9. Here, again, K1982 (HCO consumption) is stronger than K1959 (CO oxidization) at both equivalence ratios. However, the difference between the two equivalence ratios in KUCRS is smaller than that in LLNL. This applies to other C1 reactions as well. Big differences, however, exist for reactions of the H-O system. While K1932 is the strongest chain-branching reaction at $\Phi = 0.5$, it is surpassed by K1941 at $\Phi = 1.0$. As this reaction increases the reactivity of the stoichiometric case, its hot flame is located at lower wall temperatures than that of the lean case.

$$H + HO_2 \rightleftharpoons OH + OH \tag{K1941}$$

To further identify the reasons that cause the inversed reactivity trend in KUCRS, A-factor sensitivity analysis was carried out with regard to wall temperature at the hot flame position by multiplying the pre-exponential factor by 2.0 and 0.5, respectively
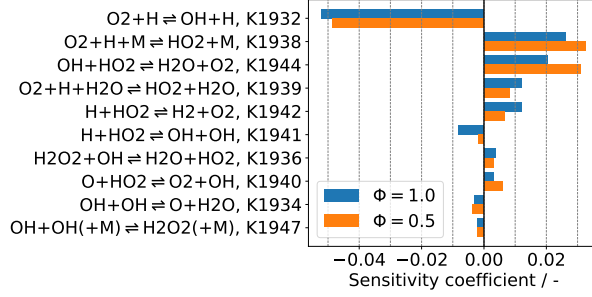
14

**Figure 10.** Sensitivity coefficients with regard to the wall temperature at the hot flame location of the ten most sensitive H-O reactions as obtained by KUCRS for PRF100 at $\Phi = 1.0$ and 0.5.

(see equation 2).

$$S = \frac{T_{\text{wall}}(k_{2.0}) - T_{\text{wall}}(k_{0.5})}{1.5 T_{\text{wall}}(k)} \qquad (2)$$

As the Arrhenius parameters for C1 reactions are the same between LLNL and KU-CRS, the sensitivity analysis focused on H-O reactions as these showed big differences between the two reaction mechanisms. The obtained sensitivity coefficients for PRF100 and KUCRS are shown in Figure 10. The reactions with the highest sensitivity at both equivalence ratios are K1932 and K1938/39. These reactions are strong competing reactions for H radicals as K1932 leads to chain branching whereas K1938/39 are chain termination reactions. K1941 and K1942 are two distinct and competing product channels of H+HO$_2$, which show high sensitivity, especially in the stoichiometric case. K1943 is another product channel but it only shows low sensitivity and is ranked 19 out of 23 in this sensitivity analysis. In the lean case, K1944, a strong chain termination reaction, shows very high sensitivity which is almost at a level with that of K1938. All of these reactions either consume H or HO$_2$.

$$\text{H} + \text{HO}_2 \rightleftharpoons \text{H}_2 + \text{O}_2 \qquad \text{(K1942)}$$

$$\text{H} + \text{HO}_2 \rightleftharpoons \text{H}_2\text{O} + \text{O} \qquad \text{(K1943)}$$

$$\text{OH} + \text{HO}_2 \rightleftharpoons \text{H}_2\text{O} + \text{O}_2 \qquad \text{(K1944)}$$

Other reactions only show small sensitivity compared with the top six reactions. Most of the top six reactions also appear among the top ten reactions just before the hot

15

flame or are competing with them for radicals, which highlights their importance for the hot flame. These results indicate that the competition between certain chain branching and chain termination reactions is the driving force behind the shift of the hot flame location. Therefore, in the next step, these reactions were investigated in more detail.

### 3.3. Impact of exchange of H-O reaction parameters

As shown in the previous section, six reactions (seven reactions, if K1943 is included as part of the $H+HO_2$ group) were identified that strongly influence the shift of the hot flame for changing equivalence ratio. For these reactions, clear differences in their numerical representation were found between the KUCRS and the LLNL mechanisms. However, K1943, which forms a group of three distinct product channels with K1941 and K1942, does not have a representation in LLNL. Therefore, in order to evaluate the impact of these reactions on the hot flame location, these seven reactions were compared with those of the *Foundational Fuel Chemistry Model* 1.0 (FFCM-1) (Smith et al., 2016). This model was chosen as it is a very recent mechanism that includes C0-C2 reactions and was optimized against a wide range of experimental and theoretical data to reduce uncertainty of the rate parameters. The Arrhenius parameters of the selected seven reactions of KUCRS and FFCM are shown in Table 2. Enhanced third-body efficiencies for reaction K1938 of both mechanisms are given in Table 3.

For reaction K1932, the Arrhenius parameters of both mechanisms are very similar. Due to FFCM's slightly higher activation energy, its rate constant is slightly lower but follows KUCRS' shape closely over the temperature range that is considered in this study (373 K to 1300 K). As this is a chain branching reaction, FFCM's lower rate constant decreases reactivity and shifts hot flames to higher temperatures (see Table 4).

In the two mechanisms, the chain termination reactions K1938/39 are expressed differently. In KUCRS, it is given as a pressure independent representation (third order reaction). Furthermore, KUCRS makes a distinction between $H_2O$ as a third body (K1939) and all other species (K1938) and is therefore split into two reactions. In FFCM (same as in LLNL), however, these reactions are combined into one and it

16

**Table 2.** Arrhenius parameters of KUCRS and FFCM of selected H-O reactions.

| Nr. | Mechanism | $A$ | $\beta$ | $E$ |
|---|---|---|---|---|
| K1932 | KUCRS | 9.756E+13 | 0.0 | 14844.6 |
|  | FFCM | 9.841E+13 | 0.0 | 15310.0 |
| K1938[1] | KUCRS | 6.300E+18 | -0.8 | 0.0 |
|  | FFCM | 4.560E+12 | 0.4 | 0.0 |
|  | - Low | 6.370E+20 | -1.72 | 525.0 |
|  | - Troe | $\alpha = 0.5,\ T^{***} = 3.0\text{E}+01$ | | |
|  |  | $T^{*} = 9.0\text{E}+04,\ T^{**} = 9.0\text{E}+04$ | | |
| K1939 | KUCRS | 6.89E+15 | 0.0 | -2086.5 |
|  | FFCM | not available | | |
| K1941 | KUCRS | 1.69E+14 | 0.0 | 874.8 |
|  | FFCM | 5.89E+13 | 0.0 | 300.0 |
| K1942 | KUCRS | 4.28E+13 | 0.0 | 1410.1 |
|  | FFCM | 2.94E+06 | 2.1 | -1455.0 |
| K1943 | KUCRS | 3.01E+13 | 0.0 | 720.8 |
|  | FFCM | 1.63E+12 | 0.0 | 0.0 |
| K1944 | KUCRS | 2.89E+13 | 0.0 | -497.1 |
|  | FFCM | 7.35E+12 | 0.0 | -1093.0 |
|  | - duplicate | 4.53E+14 | 0.0 | 10930.0 |

[1]Enhanced third-body efficiencies are given in Table 3.

is given as a Troe fall-off representation (second order reaction, compare L26) with a low-pressure limit. As these are three body reactions with enhanced third-body efficiencies, the gas composition of KUCRS of PRF100 at the hot flame location was chosen for comparison and is shown in Table 5. At $\Phi = 1.0$, the mole fractions of $N_2$ and $O_2$ are lower, whereas $H_2O$, $CO_2$ and CO mole fractions are higher. Figure 11 shows the sum of the rate constants of K1938/39 for KUCRS and the rate constant of L26 for FFCM, which were estimated using the gas composition of Table 5, over the inverse of the wall temperature range of the MFR (373 K to 1300 K). As the reaction is of third order in KUCRS, its rate constants are multiplied by the mixture's overall concentration [M]. At $\Phi = 1.0$, both mechanisms show decreasing rate constants for increasing temperatures, with that of FFCM being higher for temperatures lower than 1200 K. As this is a chain termination reaction, this leads a slightly lower reactivity of FFCM in the stoichiometric case and a shift of the hot flame to higher wall temperatures (see Table 4). At $\Phi = 0.5$, both mechanisms show lower values than for stoichiometry. These lower values can be explained by the lower concentrations of

**Table 3.** Enhanced third body efficiencies of KUCRS and FFCM for reaction K1938/L26.

| Species | KUCRS | FFCM |
|---|---|---|
| $N_2$ | 0.223 | 0.96 |
| $O_2$ | 0.123 | 0.75 |
| CO | 0.25 | 1.90 |
| $CO_2$ | 0.5 | 3.45 |
| $H_2O$ | 0.0 | 15.81 |
| He | not available | 0.71 |
| Ar | 0.0967 | 0.60 |
| $H_2$ | not available | 1.87 |
| $CH_4$ | not available | 2.00 |
| $CH_2O$ | not available | 2.50 |
| $CH_3OH$ | not available | 3.00 |
| $C_2H_6$ | not available | 3.00 |

**Table 4.** Effect of individual reactions on the wall temperature at the hot flame location when Arrhenius parameters are changed from KUCRS to FFCM for PRF100 at $\Phi = 1.0$ and 0.5.

| Reaction | $\Phi = 1.0$ | $\Phi = 0.5$ |
|---|---|---|
| K1932 | 13 K | 12 K |
| K1938/39 | 3 K | -6 K |
| K1941 | 8 K | 1 K |
| K1942 | -6 K | -3 K |
| K1943 | 0 K | 0 K |
| K1944 | -17 K | -28 K |

species with enhanced third-body efficiencies, such as CO, $CO_2$ and $H_2O$. Here, for temperatures higher than 900 K, FFCM shows a lower rate constant than KUCRS. As the chain termination reaction becomes weaker, FFCM experiences higher reactivity at lean conditions. As the difference of the rate constant between $\Phi = 1.0$ and $\Phi = 0.5$ is larger in FFCM than in KUCRS, the reactivity in FFCM is more strongly governed by this reaction than it is in KUCRS. Our previous study (Nakamura et al., 2016) showed that exhaust gas recirculation (EGR) conditions greatly influence the reactivity of the hot flame through the addition of $CO_2$ and $H_2O$ and their effect on the chain termination reactions K1938/39 (L26). This highlights the capability of the MFR to distinguish small differences in reactivity and by choosing appropriate conditions, this reaction can be studied in more detail in future studies.

Another factor for the overall reactivity is K1941, the chain branching through

**Table 5.** Species with highest mole fractions at hot flame locations of KUCRS, PRF100 at $\Phi = 1.0$ and 0.5.

| | Mole fraction | |
| Species | $\Phi = 1.0$ | $\Phi = 0.5$ |
| --- | --- | --- |
| $N_2$ | 0.721 | 0.758 |
| $O_2$ | 0.037 | 0.107 |
| $H_2O$ | 0.123 | 0.071 |
| $CO_2$ | 0.062 | 0.051 |
| CO | 0.047 | 0.012 |
| Others | 0.010 | 0.001 |
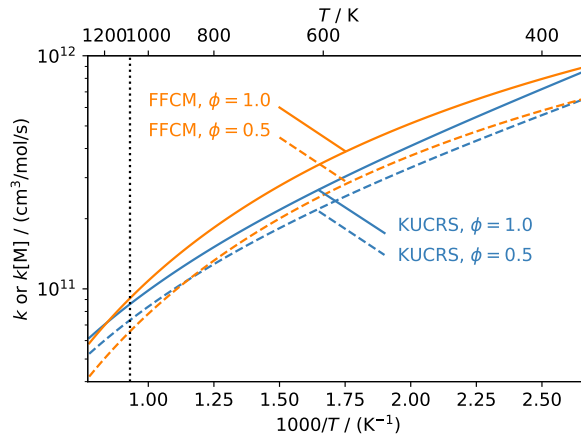


**Figure 11.** Sum of rate constants of K1938+K1939 multiplied by [M] for KUCRS and rate constant of L26 for FFCM at $\Phi = 1.0$ and 0.5. Vertical line indicates hot flame location of KUCRS for PRF100 at $\Phi = 1.0$.

H and $HO_2$ and its related reactions K1942 (chain termination) and K1943 (chain propagation). Over the whole temperature range, K1941 of FFCM has a lower rate constant than that of KUCRS, which would lead to lesser reactivity as it is a chain branching reaction. On the other hand, K1942 is also weaker in case of FFCM. As these reactions are dependent on the concentration of H and $HO_2$, they are very sensitive to the equivalence ratio and are among the most sensitive reactions in the H-O system (Burke et al., 2012). In the stoichiometric case, the change of the rate constant of K1941 decreases the hot flame reactivity and the flame shifts to higher temperatures, while the effect in the lean case is negligible (see Table 4). The change in K1942 increases the reactivity for both equivalence ratios. However, the effect in the stoichiometric case is bigger and the flame shifts more to the low temperature side than in the lean case. As K1943 is only a minor pathway that contributes less than 5% of the reaction rate within this group, its effect on the hot flame position is negligible
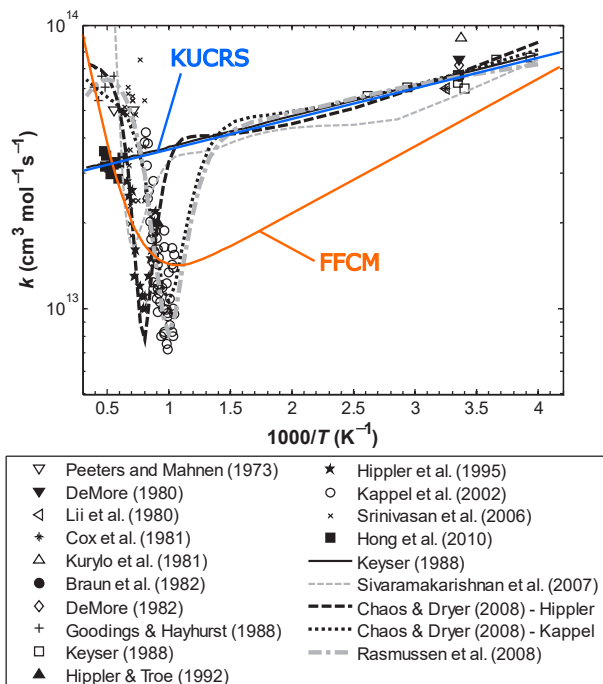
19

**Figure 12.** Rate constants of reaction K1944: OH + HO$_2$ $\rightleftharpoons$ H$_2$O + O$_2$. Symbols represent experimental data (Kappel et al., 2002; DeMore, 1979, 1982; Sridharan et al., 1984; Keyser, 1988; Lii et al., 1980; Cox et al., 1981; Kurylo et al., 1981; Braun et al., 1982; Hippler and Troe, 1992; Hippler et al., 1995; Srinivasan et al., 2006; Hong et al., 2010; Goodings and Hayhurst, 1988; Peeters and Mahnen, 1973), and lines represent proposed rate constant expressions (Keyser, 1988; Chaos and Dryer, 2008; Rasmussen et al., 2008; Sivaramakrishnan et al., 2007) as indicated in the legend. Figure taken with permission from (Burke et al., 2012) and adjusted for KUCRS and FFCM curves.

for both equivalence ratios.

Another competing reaction for HO$_2$ radicals, especially in lean conditions, is K1944, which is a chain termination reaction. The adequate numerical representation of this reaction is still controversial as experimental investigations have found a strong minimum of the rate constant at temperatures between 1000 K and 1250 K (Kappel et al., 2002; Hippler et al., 1995) (see Figure 12). This behavior was addressed theoretically by Burke et al. (Burke et al., 2013). Consistent with those results, FFCM uses a bi-Arrhenius expression for this reaction, while KUCRS does not represent the rate constant minimum. The rate constant minimum is located close to the temperature at the hot flame location (around 1070 K) and therefore this reaction has the strongest effect of all investigated reactions in this study. By introducing the FFCM representation, this reaction becomes weaker and therefore increases overall reactivity, especially in the lean case, which shifts the hot flame to lower wall temperatures by 28 K (see Table 4).
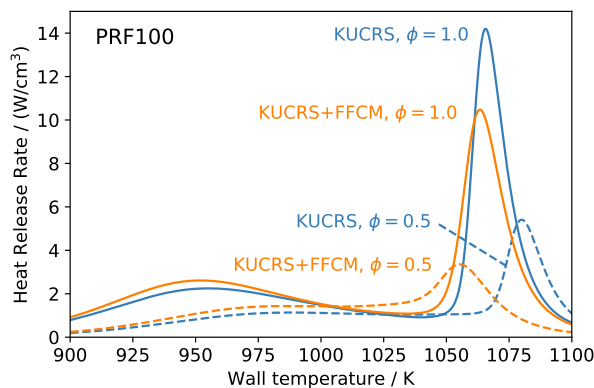
**Figure 13.** Heat release rate profiles of original KUCRS and KUCRS+FFCM for PRF100 at $\Phi = 1.0$ and 0.5.

To investigate the combined effect of the differences between KUCRS and FFCM for the selected reactions in Table 2, the Arrhenius parameters of all seven reactions of KUCRS were substituted by those of FFCM. The HRRs of the original KUCRS and KUCRS+FFCM are shown in Figure 13. At $\Phi = 1.0$, the heat release rate of KUCRS+FFCM in the blue flame follows the original very closely. The peak of the HRR of KUCRS+FFCM, however, is located at $T_{wall} = 1063\,K$, which is $2\,K$ lower than the original result. More pronounced changes are found at $\Phi = 0.5$. Here, starting in the blue flame, the HRR of KUCRS+FFCM shows a slightly bigger increase. This leads to a hot flame at $25\,K$ lower wall temperature than the original mechanism, with the HRR peak shifting from $1080\,K$ to $1055\,K$. These changes to the heat release rates effectively lead to an inversion of the reactivity trend for decreasing equivalence ratio, i.e., higher reactivity of the hot flame for leaner conditions. The difference of the wall temperature at the hot flame location for $\Phi = 1.0$ and 0.5 for KUCRS+FFCM now is $8\,K$, which agrees very well with the experimental results. The results of the wall temperatures at the hot flame location obtained by KUCRS+FFCM for all nine investigated cases are compared with the experimental results and those obtained by the original KUCRS and LLNL in Figure 14. In this figure it can be seen that for KUCRS+FFCM, the hot flames of all three fuels shift to lower wall temperatures for decreasing equivalence ratio. Furthermore, the shift to lower wall temperatures for decreasing RON is reproduced very well. The agreement of KUCRS+FFCM with the experimental results is within $8\,K$, which is better than that of LLNL.

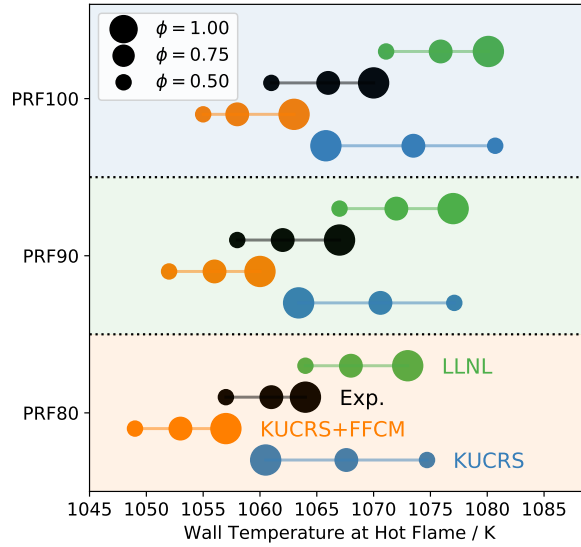The effect of the substitution of H-O reactions by those of FFCM on the mole

**Figure 14.** Wall temperature at hot flame location for all investigated cases, experiments and simulations including KUCRS+FFCM.
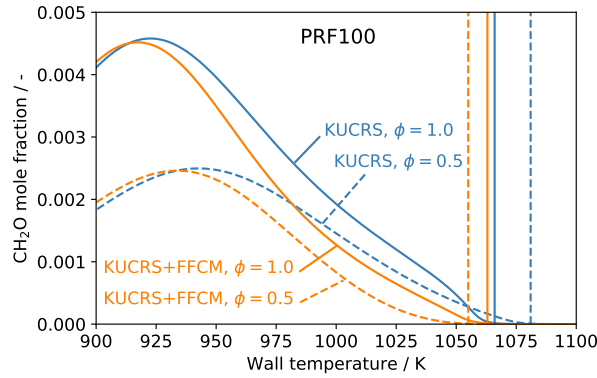


**Figure 15.** $CH_2O$ mole fraction profiles of original KUCRS and KUCRS+FFCM of PRF100 at $\Phi = 1.0$ and 0.5. Vertical lines represent the hot flame location of each case.

fraction profile of an important intermediate species, $CH_2O$, is shown in Figure 15. As mentioned before, $CH_2O$ is consumed in the blue flame. This is in accordance with the mole fraction profiles of Figure 15, where the hot flames are found at locations where the $CH_2O$ mole fraction approaches zero. At $\Phi = 1.0$, KUCRS shows higher values compared with the modified mechanism. Just before the hot flame (around 1050 K), however, it experiences a sharp decrease and drops below the values of the lean case. This indicates that the blue flame is influenced by the hot flame in the stoichiometric case. This interaction of the blue flame and the hot flame increases the reactivity and leads, in turn, to a hot flame at lower wall temperature, which is opposite to the
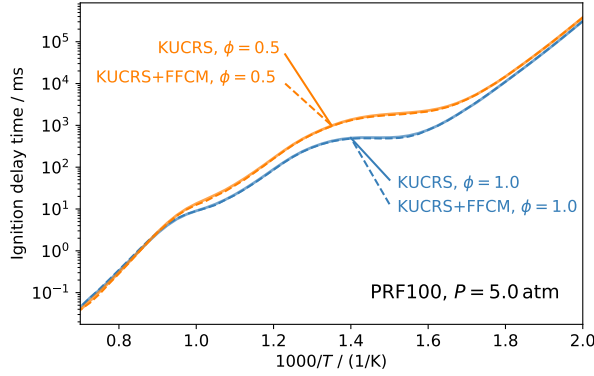
**Figure 16.** Ignition delay times of original KUCRS and KUCRS+FFCM for PRF100 at $P = 5\,\text{atm}$, $\Phi = 1.0$ and 0.5.

experimental results. Through the substitution of H-O reactions by FFCM, $CH_2O$ is consumed at slightly lower wall temperatures for both equivalence ratios. This leads to a better spatial separation of the blue flame and the hot flame in the stoichiometric case, which in turn leads to a smoother decrease of the $CH_2O$ profile near the hot flame without the sharp drop.

### 3.4. Validation by ignition delay times and laminar burning velocities

To investigate the applicability of KUCRS+FFCM in other investigation methods, such as ignition delay times in shock tubes, zero-dimensional simulations were conducted with Chemkin-Pro Aurora (ANSYS, 2016). Adiabatic, constant-volume ignition delay times were computed over a temperature range of $500\,\text{K}$ to $1428\,\text{K}$ at $5\,\text{atm}$, as this pressure is similar to that of spark ignition at lean conditions in an IC engine. The resulting graphs for PRF100 at $\Phi = 1.0$ and 0.5 of the original KUCRS and KUCRS+FFCM are shown in Figure 16. Over the whole temperature range, ignition delay times of KUCRS+FFCM are almost identical with those of the original mechanism. The reason for this agreement is that under adiabatic ignition conditions, chemical reactions proceed rapidly with strong heat release and are not affected by small changes to the H-O system. On the other hand, chemical reactions in the MFR proceed gradually with mild heat release under well-controlled temperature conditions. As a result, the MFR system is considered to show the reaction competition between chain branching and chain termination more clearly than the adiabatic ignition system.

23

Another widely used method is the measurement and the calculation of laminar burning velocities. To compare the performance of KUCRS+FFCM with the base mechanism, one-dimensional computations were conducted by Chemkin-Pro PRE-MIX (ANSYS, 2016). At atmospheric pressure, the differences between the original KUCRS and KUCRS+FFCM were less than 2 % at equivalence ratios between 0.7 and 1.1, which shows excellent agreement.

These results indicate that the micro flow reactor with a controlled temperature profile offers insight into interactions between reactions that are not possible by conventional investigation methods. By using the MFR method, it is therefor expected that further improvements of existing reaction mechanisms can be achieved. Therefore, as a next step, MFR experiments at elevated pressures will be conducted to investigate the equivalence ratio dependence of fuel reactivity at conditions of practical ultra-lean gasoline engines.

## 4. Conclusions

In this study, a vertical-type micro flow reactor with a controlled temperature profile was used to investigate the reactivity of ultra-lean PRF/air weak flames experimentally. 1-D steady computations with heat transfer between the wall and the gas-phase were conducted to analyze occurring chemical reactions in high detail. The following observations were made:

(1) In the experiments, separated blue and hot flames were obtained. As the equivalence ratio was decreased, the hot flames shifted to lower wall temperatures, indicating higher reactivity.

(2) Computation with LLNL and KUCRS reaction mechanisms showed HRR-zones for the blue and hot flames. However, only LLNL was able to reproduce the increasing reactivity for lower equivalence ratio, while KUCRS showed the opposite trend. In LLNL, the region of the consumption of intermediate species, the blue flame, and the region of CO oxidization and H-O reactions, the hot flame, were well separated. Therefore, the hot flame was governed by H-O reactions, which increased the reactivity at $\Phi = 0.5$ through high temperature chain branching

24

by $O_2 + H \rightleftharpoons OH + O$. In KUCRS, however, a spatial overlap of the blue flame and the hot flame lead to increased chain branching and a higher reactivity at $\Phi = 1.0$.

(3) By comparing essential reactions at stoichiometric and lean conditions for the two mechanisms, as well as conducting sensitivity analysis with regard in the hot flame location, seven essential H-O reactions were identified. These reactions are competing chain branching and chain termination reactions. By substituting these seven reactions in KUCRS by those of the FFCM model, the reactivity trend was inversed and agreed well with the experimental results. The applicability of this modified mechanism was verified by simulations of ignition delay times and laminar burning velocities, which were in excellent agreement with the original mechanism.

## 5. Declaration of conflicting interests

The authors declared no potential conflicts of interest with respect to the research, authorship and/or publication of this article.

## 6. Funding

## References

AlAbbad, M., Javed, T., Khaled, F., Badra, J., and Farooq, A. 2017. Ignition delay time measurements of primary reference fuel blends. *Combust. Flame*, **178**, 205–216.

Andrae, J., Björnbom, P., Cracknell, R., and Kalghatgi, G. 2007. Autoignition of toluene reference fuels at high pressures modeled with detailed chemical kinetics. *Combust. Flame*, **149**(1-2), 2–24.

ANSYS, I. 2016. *CHEMKIN-PRO 17.2.* San Diego.

Bradley, D., Lawes, M., and Sheppard, C. G. W. 2000. Combustion and the thermodynamic performance of spark ignition engines. *Proc. Instn. Mech. Engrs. C*, **214**(1), 257–268.

Braun, M., Hofzumahaus, A., and Stuhl, F. 1982. VUV Flash Photolysis Study of the Reaction of HO with HO2 at 1 atm and 298 K. *Ber. Bunsen Ges. Phys. Chem.*, **86**(7), 597–602.

Burke, M. P., Chaos, M., Ju, Y., Dryer, F. L., and Klippenstein, S. J. 2012. Comprehensive H2/O2 kinetic model for high-pressure combustion. *Int. J. Chem. Kinet.*, **44**(7), 444–474.

Burke, M. P., Klippenstein, S. J., and Harding, L. B. 2013. A quantitative explanation for the apparent anomalous temperature dependence of OH+HO2=H2O+O2 through multi-scale modeling. *Proc. Combust. Inst.*, **34**(1), 547–555.

Chaos, M., and Dryer, F. L. 2008. Syngas Combustion Kinetics and Applications. *Combust. Sci. Technol.*, **180**(6), 1053–1096.

Chen, B., Togbé, C., Selim, H., Dagaut, P., and Sarathy, S. M. 2017. Quantities of Interest in Jet Stirred Reactor Oxidation of a High-Octane Gasoline. *Energy Fuels*, **31**(5), 5543–5553.

Cox, R., Burrows, J., and Wallington, T. 1981. Rate coefficient for the reaction OH + HO2 = H2O + O2 at 1 atmosphere pressure and 308 K. *Chem. Phys. Lett.*, **84**(2), 217–221.

Curran, H., Gaffuri, P., Pitz, W., and Westbrook, C. 2002. A comprehensive modeling study of iso-octane oxidation. *Combust. Flame*, **129**(3), 253–280.

DeMore, W. B. 1979. Reaction of hydroperoxo radicals with ozone and the effect of water vapor on hydroperoxo kinetics. *J. Phys. Chem.*, **83**(9), 1113–1118.

DeMore, W. B. 1982. Rate constant and possible pressure dependence of the reaction hydroxyl + hydroperoxo. *J. Phys. Chem.*, **86**(1), 121–126.

Di Stazio, A., Chauveau, C., Dayma, G., and Dagaut, P. 2016. Combustion in micro-channels with a controlled temperature gradient. *Exp. Therm Fluid Sci.*, **73**, 79–86.

Gauthier, B., Davidson, D., and Hanson, R. 2004. Shock tube determination of ignition delay times in full-blend and surrogate fuel mixtures. *Combust. Flame*, **139**(4), 300–311.

Goodings, J. M., and Hayhurst, A. N. 1988. Heat release and radical recombination in premixed fuel-lean flames of H2+O2+N2. Rate constants for H + OH + M -> H2O + M and HO2+ OH -> H2O + O2. *J. Chem. Soc., Faraday Trans. 2*, **84**(6), 745.

Hartmann, M., Gushterova, I., Fikri, M., Schulz, C., Schießl, R., and Maas, U. 2011. Auto-ignition of toluene-doped n-heptane and iso-octane/air mixtures: High-pressure shock-tube experiments and kinetics modeling. *Combust. Flame*, **158**(1), 172–178.

Hippler, H., Neunaber, H., and Troe, J. 1995. Shock wave studies of the reactions HO+H2O2=>H2O+HO2 and HO+HO2=>H2O+O2 between 930 and 1680 K. *J. Chem. Phys.*, **1031**(129), 1755–14506.

Hippler, H., and Troe, J. 1992. Rate constants of the reaction HO+H2O2->HO2+H2O at T>1000 K. *Chem. Phys. Lett.*, **192**(4), 333–337.

Hong, Z., Vasu, S. S., Davidson, D. F., and Hanson, R. K. 2010. Experimental Study of the Rate of OH + HO2 -> H2O + O2 at High Temperatures Using the Reverse Reaction. *J. Phys. Chem. A*, **114**(17), 5520–5525.

Hori, M., Nakamura, H., Tezuka, T., Hasegawa, S., and Maruta, K. 2013. Characteristics of n-heptane and toluene weak flames in a micro flow reactor with a controlled temperature profile. *Proc. Combust. Inst.*, **34**(2), 3419–3426.

Hori, M., Yamamoto, A., Nakamura, H., Tezuka, T., Hasegawa, S., and Maruta, K. 2012. Study on octane number dependence of PRF/air weak flames at 1-5 atm in a micro flow reactor with a controlled temperature profile. *Combust. Flame*, **159**(3), 959–967.

Javed, T., Lee, C., AlAbbad, M., Djebbi, K., Beshir, M., Badra, J., ... Farooq, A. 2016. Ignition studies of n-heptane/iso-octane/toluene blends. *Combust. Flame*, **171**, 223–233.

Kamada, T., Nakamura, H., Tezuka, T., Hasegawa, S., and Maruta, K. 2014. Study on combustion and ignition characteristics of natural gas components in a micro flow reactor with a controlled temperature profile. *Combust. Flame*, **161**(1), 37–48.

Kappel, C., Luther, K., and Troe, J. 2002. Shock wave study of the unimolecular dissociation of H2O2 in its falloff range and of its secondary reactions. *Phys. Chem. Chem. Phys.*, **4**(18), 4392–4398.

Keyser, L. F. 1988. Kinetics of the reaction hydroxyl + hydroperoxo => water + oxygen from 254 to 382 K. *J. Phys. Chem.*, **92**(5), 1193–1200.

Kikui, S., Kamada, T., Nakamura, H., Tezuka, T., Hasegawa, S., and Maruta, K. 2015. Characteristics of n-butane weak flames at elevated pressures in a micro flow reactor with a controlled temperature profile. *Proc. Combust. Inst.*, **35**(3), 3405–3412.

Kikui, S., Nakamura, H., Tezuka, T., Hasegawa, S., and Maruta, K. 2016. Study on combustion and ignition characteristics of ethylene, propylene, 1-butene and 1-pentene in a micro flow reactor with a controlled temperature profile. *Combust. Flame*, **163**, 209–219.

Kizaki, Y., Nakamura, H., Tezuka, T., Hasegawa, S., and Maruta, K. 2015. Effect of radical quenching on CH4/air flames in a micro flow reactor with a controlled temperature

profile. *Proc. Combust. Inst.*, **35**(3), 3389–3396.

Kukkadapu, G., Kumar, K., Sung, C.-J., Mehl, M., and Pitz, W. J. 2012. Experimental and surrogate modeling study of gasoline ignition in a rapid compression machine. *Combust. Flame*, **159**(10), 3066–3078.

Kukkadapu, G., Kumar, K., Sung, C.-J., Mehl, M., and Pitz, W. J. 2015. Autoignition of gasoline surrogates at low temperature combustion conditions. *Combust. Flame*, **162**(5), 2272–2285.

Kurylo, M. J., Klais, O., and Laufer, A. H. 1981. Mechanistic investigation of the hydroxyl + hydroperoxo reaction. *J. Phys. Chem.*, **85**(24), 3674–3678.

Li, X., Jia, L., Nakamura, H., Tezuka, T., Hasegawa, S., and Maruta, K. 2015. Study on flame responses and ignition characteristics of CH4/O2/CO2 mixture in a micro flow reactor with a controlled temperature profile. *Appl. Therm. Eng.*, **84**, 360–367.

Lii, R.-R., Gorse, R. A., Sauer, M. C., and Gordon, S. 1980. Temperature dependence of the gas-phase self-reaction of hydroperoxo radicals in the presence of ammonia. *J. Phys. Chem.*, **84**(8), 813–817.

Maruta, K., Kataoka, T., Kim, N. I., Minaev, S., and Fursenko, R. 2005. Characteristics of combustion in a narrow channel with a temperature gradient. *Proc. Combust. Inst.*, **30**(2), 2429–2436.

Mehl, M., Pitz, W. J., Westbrook, C. K., and Curran, H. J. 2011. Kinetic modeling of gasoline surrogate components and mixtures under engine conditions. *Proc. Combust. Inst.*, **33**(1), 193–200.

Minaev, S., Maruta, K., and Fursenko, R. 2007. Nonlinear dynamics of flame in a narrow channel with a temperature gradient. *Combust. Theor. Model.*, **11**(2), 187–203.

Miyoshi, A. 2011. Systematic Computational Study on the Unimolecular Reactions of Alkyl-peroxy (RO2), Hydroperoxyalkyl (QOOH), and Hydroperoxyalkylperoxy (O2QOOH) Radicals. *J. Phys. Chem. A*, **115**(15), 3301–3325.

Miyoshi, A., and Sakai, Y. 2017. Construction of the gasoline surrogate detailed reaction mechanism. In *JSAE annual congress spring*.

Nakamura, H., Takahashi, H., Tezuka, T., Hasegawa, S., Maruta, K., and Abe, K. 2016. Effects of CO-to-H2 ratio and diluents on ignition properties of syngas examined by weak flames in a micro flow reactor with a controlled temperature profile. *Combust. Flame*, **172**, 94–104.

Nakamura, H., Yamamoto, A., Hori, M., Tezuka, T., Hasegawa, S., and Maruta, K. 2013. Study

on pressure dependences of ethanol oxidation by separated weak flames in a micro flow reactor with a controlled temperature profile. *Proc. Combust. Inst.*, **34**(2), 3435–3443.

Okuno, T., Nakamura, H., Tezuka, T., Hasegawa, S., and Maruta, K. 2017. Ultra-lean combustion characteristics of premixed methane flames in a micro flow reactor with a controlled temperature profile. *Proc. Combust. Inst.*, **36**(3), 4227–4233.

Oshibe, H., Nakamura, H., Tezuka, T., Hasegawa, S., and Maruta, K. 2010. Stabilized three-stage oxidation of DME/air mixture in a micro flow reactor with a controlled temperature profile. *Combust. Flame*, **157**(8), 1572–1580.

Peeters, J., and Mahnen, G. 1973. Reaction mechanisms and rate constants ofelementary steps in methane-oxygen flames. *Symp. (Int.) Combust.*, **14**(1), 133–146.

Rasmussen, C. L., Hansen, J., Marshall, P., and Glarborg, P. 2008. Experimental measurements and kinetic modeling of CO/H2/O2/NOx conversion at high pressure. *Int. J. Chem. Kinet.*, **40**(8), 454–480.

Saiki, Y., Fan, Y., and Suzuki, Y. 2015. Radical quenching of metal wall surface in a methane-air premixed flame. *Combust. Flame*, **162**(10), 4036–4045.

Saiki, Y., and Suzuki, Y. 2013. Effect of wall surface reaction on a methane-air premixed flame in narrow channels with different wall materials. *Proc. Combust. Inst.*, **34**(2), 3395–3402.

Sarathy, S. M., Kukkadapu, G., Mehl, M., Wang, W., Javed, T., Park, S., ... Sung, C.-J. 2015. Ignition of alkane-rich FACE gasoline fuels and their surrogate mixtures. *Proc. Combust. Inst.*, **35**(1), 249–257.

SIP. 2015. *SIP Pioneering the Future: Japanese Science, Technology and Innovation 2015.* Retrieved from `http://www8.cao.go.jp/cstp/panhu/sip_english/sip_en.html`

Sivaramakrishnan, R., Comandini, A., Tranter, R., Brezinsky, K., Davis, S., and Wang, H. 2007. Combustion of CO/H2 mixtures at elevated pressures. *Proc. Combust. Inst.*, **31**(1), 429–437.

Smith, G., Tao, Y., and Wang, H. 2016. *Foundational Fuel Chemistry Model Version 1.0 (FFCM-1).* Retrieved 2017-11-30, from `http://nanoenergy.stanford.edu/ffcm1`

Sridharan, U. C., Qiu, L. X., and Kaufman, F. 1984. Rate constant of the hydroxyl + perhydroxyl (HO2) reaction from 252 to 420 K. *J. Phys. Chem.*, **88**(7), 1281–1282.

Srinivasan, N. K., Su, M.-C., Sutherland, J. W., Michael, J. V., and Ruscic, B. 2006. Reflected Shock Tube Studies of High-Temperature Rate Constants for OH + NO2 -> HO2 + NO and OH + HO2 -> H2O + O2. *J. Phys. Chem. A.*, **110**(21), 6602–6607.

Tsuboi, Y., Yokomori, T., and Maruta, K. 2009. Lower limit of weak flame in a heated channel. *Proc. Combust. Inst.*, **32**(2), 3075–3081.

Yamamoto, A., Oshibe, H., Nakamura, H., Tezuka, T., Hasegawa, S., and Maruta, K. 2011. Stabilized three-stage oxidation of gaseous n-heptane/air mixture in a micro flow reactor with a controlled temperature profile. *Proc. Combust. Inst.*, **33**(2), 3259–3266.